# *Effect of redox conditions on sulfur and selenium binding in AFm phases*

Latina Nedyalkova[1,2*], Barbara Lothenbach[2], Jan Tits[1], Erich Wieland[1], Urs Mäder[3]

[1] Paul Scherrer Institute, Laboratory for Waste Management (CH)
[2] Empa, Laboratory for Concrete & Construction Chemistry (CH)
[3] Institute of Geological Sciences, University of Bern (CH)

* Corresponding author: latina.nedyalkova@psi.ch

## Abstract

The incorporation of Se and S in AFm phases was investigated. Se(VI)-, Se(IV)-, S(VI)-, S(IV)- and S(II)-AFm phases were synthesized accounting for a range of redox conditions representative of a cement-based L/ILW repository. The AFm phases were characterized by TGA, FTIR and X-ray diffraction. From bulk chemical analysis of the liquid phase and the pH values, the solubility products were determined. Furthermore, the effect of the equilibration time (3 months *vs.* 6 months) and pH (higher pH of ~ 13 *vs.* lower pH of ~ 12) on the stability of the phases was examined.

The X-ray spectra revealed crystalline phases with rhombohedral and monoclinic structure. For the phases with rhombohedral structure different interlayer distances (hkl 003 and 006) were observed, whereas no shift of the reflection referring to the main layer (hkl 110) could be detected. The TGA analyses showed typical water loss patterns for AFm phases giving total water contents of 11 $H_2O$ molecules for the S(IV)- and the Se(IV)-AFm, 12 $H_2O$ molecules for the S(VI)-AFm and 13 $H_2O$ molecules for the S(II)- and Se(VI)-AFm. The variations in the crystal symmetry and the basal spacing seem to be a function of the size of the interlayer atoms and/or the number of water molecules. These observations suggest an intercalation of the Se and S anions in the AFm interlayers.

## Introduction

One concept for radioactive waste management foresees the disposal of low- and intermediate level nuclear waste (L/ILW) in deep geological repositories. Cementitious materials are used for the solidification of the waste and for the construction of the engineered barrier system whose function is among others to retard the mobility of the radionuclides in the repository near-field. Under the alkaline and reducing conditions prevailing in such repositories many common near- and far-field minerals carry negatively charged surfaces which efficiently retard cationic radionuclides. Radionuclides with anionic speciation, such as selenium, however, are expected to be only weakly retarded. Potential anionic exclusion could decrease the effective diffusion coefficient of anions compared to diffusion coefficient of cations. Nevertheless, due to its long half-life, selenium is defined as an important dose-determining radionuclide in L/ILW repositories (Nagra, 2002).

Safety assessment so far did not take fully into consideration the potential uptake by some positively charged anion exchangers present in the cementitious near-field matrix, such as AFm($Al_2O_3$-$Fe_2O_3$-mono) phases. AFm phases belong to the layered double hydroxides (LDH) and form during the hydration of cement. They have a lamellar structure with a positively charged main layer, $[Ca_4(Al,Fe)_2(OH)_{12}]^+$, and a negatively charged interlayer, $[X \cdot nH_2O]^{2-}$, where X denotes two singly charged or a doubly charged anion. The main layers consist of sheets of

$Ca(OH)_6$ octahedra with every third $Ca^{2+}$ site being occupied by $Al^{3+}$ and/or $Fe^{3+}$, generating thus a positive net charge. Different charge balancing anions and different numbers of water molecules can be present in the interlayer. The anions typically found in AFm phases are $OH^-$, $SO_4^{2-}$, $Cl^-$ and $CO_3^{2-}$ forming hydroxyl-AFm, monosulfate, Friedel's salt, hemi- and monocarbonate, respectively (Evans and Slade, 2006).

Under the alkaline conditions (10 < pH 13.5) in a cement-based repository Se will be present in anionic form and may exchange for the common interlayer anions. The aqueous speciation is dominated by $SeO_4^{2-}$ (Se(VI), selenate) under oxidizing conditions and $SeO_3^{2-}$ (Se(IV), selenite ion), $HSe^-$ (Se(-II), selenide) and a series of polyselenides ($Se_x^{2-}$, x = 2, 3, 4) under reducing conditions (Olin et al., 2005) (Figure 1). In addition, reduced anionic species of S, namely $SO_3^{2-}$ (S(IV), sulfite), $S_2O_3^{2-}$ (S(II), thiosulfate) and $HS^-$ (S(-II), sulfide), may also be present as competitive anions for the AFm interlayer sites.

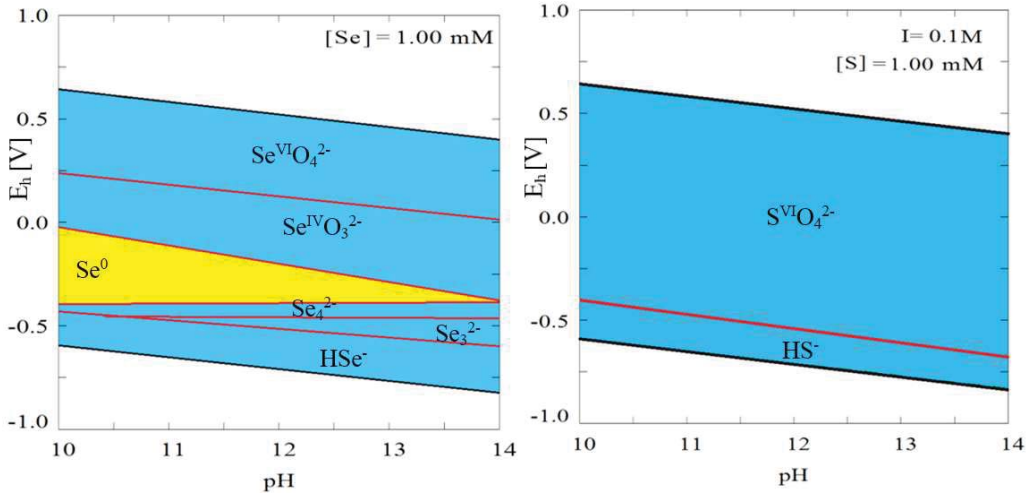


***Figure 1:*** *Predominance diagram for selenium (left) and sulfur (right) in the pH and Eh regions relevant for the cementitious near field of a L/ILW repository; the reduced sulfur species $SO_3^{2-}$ and $S_2O_3^{2-}$ are thermodynamically metastable relative to the main species $SO_4^{2-}$ and $HS^-$ and are therefore not visible on a predominance diagram. Calculations were performed using the code Medusa (Puigdomenech, 1983) and thermodynamic data from the NEA thermodynamic database.*

As AFm phases have the potential to bind Se in their structure and may play an important role in the immobilization of this hazardous element, a thorough understanding of the incorporation of selenium and sulfur in AFm phases is required. The binding of S(VI) in AFm phases and its structure are very well investigated. The S(VI)-AFm has a rhombohedral structure belonging to the $R\bar{3}$ space group (Allmann, 1977). The S(IV)-AFm phase has been synthesized and characterized before (Motzet and Pöllmann, 1999) but no solubility measurements or thermodynamic data for it are available. Data for the more reduced sulfur species S(II) and S(-II) are completely missing, although their existence has been suggested (Vernet, 1982). Similarly for Se: several studies deal with the Se(VI) and Se(IV) uptake by AFm phases (e.g., Baur and Johnson, 2003a; Bonhoure et al., 2006; Mace et al., 2007), while data for Se(-II) are still missing.

The objective of this study is to further investigate the incorporation of selenium and sulfur in AFm phases and work towards the construction of a thermodynamic model describing the uptake. For this purpose, pure Se(VI)-, Se(IV)-, S(VI)-, S(IV)-, S(II)-AFm phases were synthesized, accounting for a range of possible redox conditions in a cement-based repository in deep geological formations. The AFm phases were characterized by various techniques (XRD, TGA, FTIR, Raman, aqueous phase analysis) and their solubility products calculated.

## Results and discussion

### *Characteristics of the synthesized AFm phases*

Five different AFm phases were synthesized: $SO_4$-, $SeO_4$-, $SO_3$-, $SeO_3$- and $S_2O_3$-AFm, using $C_3A$, CaO and $Na_2$-salts as starting materials (pH ~ 13). After three months of equilibration time, the samples were filtered and dried in a desiccator over a saturated NaOH solution (~ 10% relative humidity) at room temperature for five to six weeks.

#### *TGA*

The TGA-DTG curves show a typical water loss pattern for AFm with total mass losses of ~ 34.5 wt.% for the $SO_4$-AFm, between 33.0 and 33.2 wt.% for the $SO_3$- and $S_2O_3$-AFm, ~ 32.3 wt.% for $SeO_4$-AFm and ~ 31.2 wt.% for $SeO_3$-AFm (Figure 2). The water removal occurs in several steps: up to 250°C the loosely bound water in the interlayer is lost, while at temperatures between 250 - 500°C water in the main layer is lost. The total amount of water estimated is ~ 11 $H_2O$ for the $SO_3$- and $SeO_3$-AFm phases, ~ 12 $H_2O$ for the $SO_4$-AFm, and ~ 13 $H_2O$ for the $S_2O_3$- and $SeO_4$-AFm phases. All synthesized AFm phases contain ~ 6 $H_2O$ in the main layer.

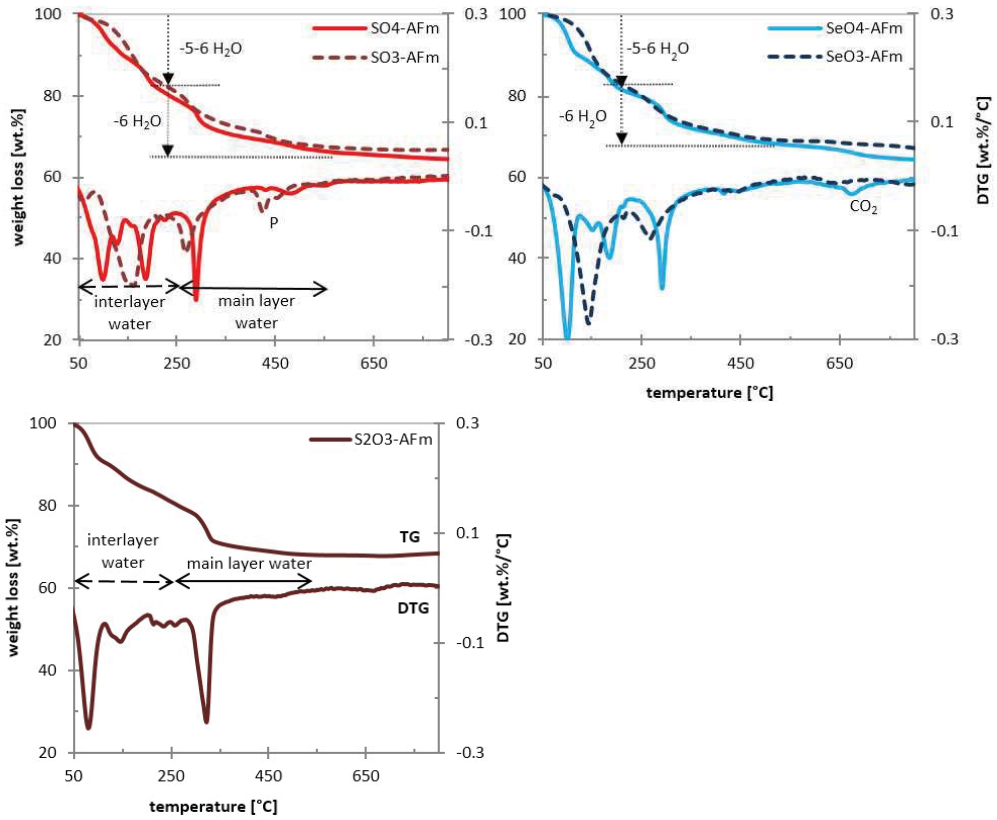


***Figure 2:*** *TGA and DTG curves of the synthesized AFm phases (pH ~ 13) after 3 months equilibration time and drying over a saturated NaOH solution (r.h. ~ 10%). P: portlandite.*

#### *XRD*

The XRD-patterns show that well-crystalline AFm phases have formed (Figure 3). Comparison of all synthesized samples, however, indicates that the $SeO_3$- and the $S_2O_3$-AFm are somewhat less crystalline with less

clearly defined peaks. Impurities such as ettringite (Et) in the $SO_4$-AFm, portlandite (P) in the $SeO_4$- and $SeO_3$-AFm, hemicarbonate in the $S_2O_3$- and $SeO_4$-AFm, as well as some katoite (K) in the $SeO_3$-AFm were also detected. Evidence for the rhombohedral structure of the $SO_4$-AFm comes from the main layer peak (hkl 110) at 31° 2θ. In addition, its two main diffraction peaks are at 9.9° and 19.9° 2θ corresponding to Miller indices (003) and (006) and d-values of 8.93 Å and 4.47 Å, respectively (Allmann, 1977). Depending on the exposure temperature and relative humidity, several hydration states of $SO_4$-AFm can exist - Ms9, Ms10.5, Ms12 and Ms14 (with the index number giving the water content of the phase in moles), each characterized by different interlayer distances (Baquerizo et al., 2015). Although the main hydration state observed here is Ms12, the additional peaks left of the (hkl 003) and (hkl 006) reflexions indicate also the presence of minor Ms14 which is most probably the result of insufficient drying.

The $SO_3$- and $SeO_3$-AFm phases exhibit the same main layer peak (hkl 110) at 2θ ~ 31° indicating also a rhombohedral structure. The $SO_3$-AFm is characterized by higher 2θ values and hence smaller basal spacings (hkl 003 and 006), consistent with the presence of less water in the interlayer space and smaller anionic size. Although the XRD pattern of the $S_2O_3$-AFm appears to be similar to those of the $SO_4$- and the $SO_3$-AFm, it has an additional diffraction peak at ~ 11° 2θ which cannot be explained by a rhombohedral symmetry and is more consistent to a monoclinic structure. Similarly, the numerous diffraction peaks of the $SeO_4$-AFm pattern indicate a lower, also monoclinic symmetry. The crystal structure analyses for the $SO_3$-, $S_2O_3$-, $SeO_4$- and $SeO_3$-AFm phases are still ongoing and the correct structure symmetries of the phases are yet to be specified.

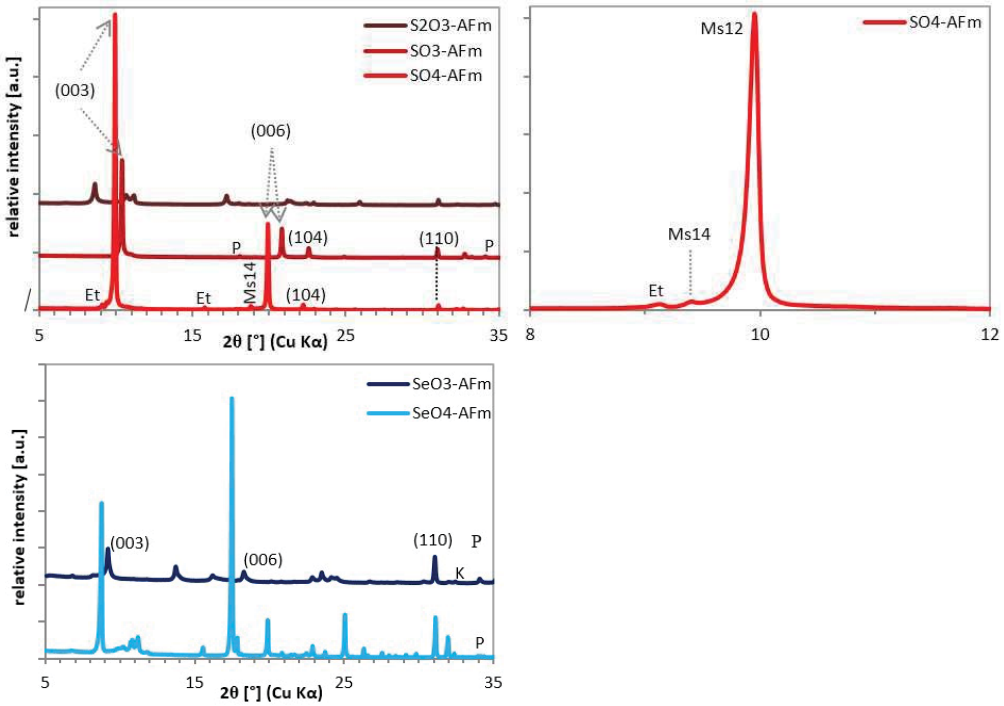


***Figure 3:*** *XRD-pattern of the synthesized AFm phases (pH ~ 13) after 3 months equilibration time and drying over a saturated NaOH solution (r.h. ~ 10%); the image on the top right shows the (003)-peak area of the $SO_4$-AFm in details. Et: ettringite; Ms: monosulfate; K: katoite.*

*FTIR/Raman spectra*

The IR-spectra (Figure 4 and Table 1) of the synthesized samples indicate two different types of hydrous components. The broad band in the 3,600 - 3,000 $cm^{-1}$ region as well as the absorption band at approximately

1,650 - 1,600 $cm^{-1}$ is caused by $H_2O$ from the interlayer, while an absorption at ~ 3,670 - 3,650 $cm^{-1}$ is characteristic of a single hydroxyl group. Generally, sharp peaks between 3,600 and 3,000 $cm^{-1}$ indicate more highly coordinated interlayer water (Dilnesa et al., 2011). The IR-spectra show better ordered water in the $SO_4$-, $SeO_4$- and $S_2O_3$-AFm phases; whereas in the $SO_3$- and the $SeO_3$-AFm less ordering can be observed. All samples show minor $CO_2$-contamination, visible by a band at 1,450 - 1,250 $cm^{-1}$. IR measurements were also carried out on the $Na_2$-X salts used for the synthesis in order to verify the peak positions of the main anions.

Raman spectra are plotted against the IR spectra on Figure 4 for comparison. Both spectra show similar patterns. The band position for $Al(OH)_6$ appears at ~ 532 $cm^{-1}$; the S-O and Se-O vibrations occur between ~ 970 - 980 $cm^{-1}$ for $SO_3$ and $SO_4$, and between ~ 793 - 832 $cm^{-1}$ for $SeO_3$ and $SeO_4$. Small bands at ~ 1,085 $cm^{-1}$ belong to weakly bound carbonate due to $CO_2$ contamination. The hydrogen bond network vibrations can be seen in the range ~ 2,800 - 4,000 $cm^{-1}$. A broad band at the beginning of this range can be attributed to $H_2O$, while a sharper signal at the end (~ 3,688 $cm^{-1}$) results from the presence of OH groups (Renaudin et al., 2007).

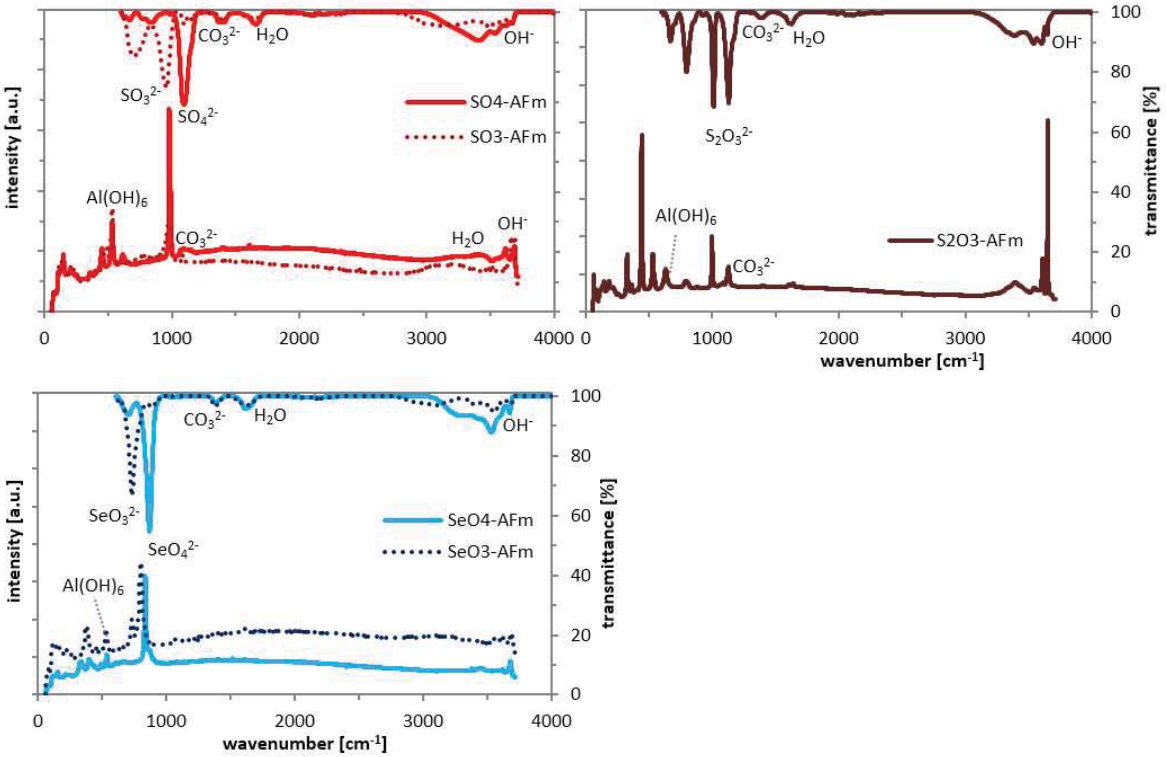


***Figure 4:*** *FTIR (top) and Raman (bottom) spectra of the synthesized AFm phases (pH ~ 13) after 3 months equilibration time and drying over a saturated NaOH solution (r.h. ~ 10%).*

***Table 1:*** *Vibrations in the IR spectra of the synthesized AFm-phases (Dilnesa et al., 2011).*

| Wave number [$cm^{-1}$] | Vibration | Wave number [$cm^{-1}$] | Vibration |
|---|---|---|---|
| 480 - 960 | Al-O, Ca-OH | 1,250 - 1,450 | $CO_2$ |
| ~ 735 | $SeO_3^{2-}$ | 1,600 - 1,650 | $v_2$-$H_2O$ |
| ~ 874 | $SeO_4^{2-}$ | 3,000 - 3,600 | $H_2O$ interlayer |
| ~ 955 | $v_3$-$SO_3^{2-}$ | 3,650 - 3,670 | OH main layer |
| ~ 1,105 | $v_1$-$SO_4^{2-}$ | | |

### *Effect of equilibration time*

The five AFm phases were also analysed after longer equilibration times, i.e., after 6 months. The XRD-patterns of the 6 month samples (Figure 5) show no notable mineralogical changes; some of the AFm phases, however, display sharper peaks and higher intensities (in particular $S_2O_3$-AFm) indicating better ordering and/or an increase in the number of layers stacked. The $SeO_4$-AFm has an additional peak next to the (003)-reflex (MSe10) indicating the presence of an $SeO_4$-AFm phase containing 10 $H_2O$ molecules, which is the result of longer drying.

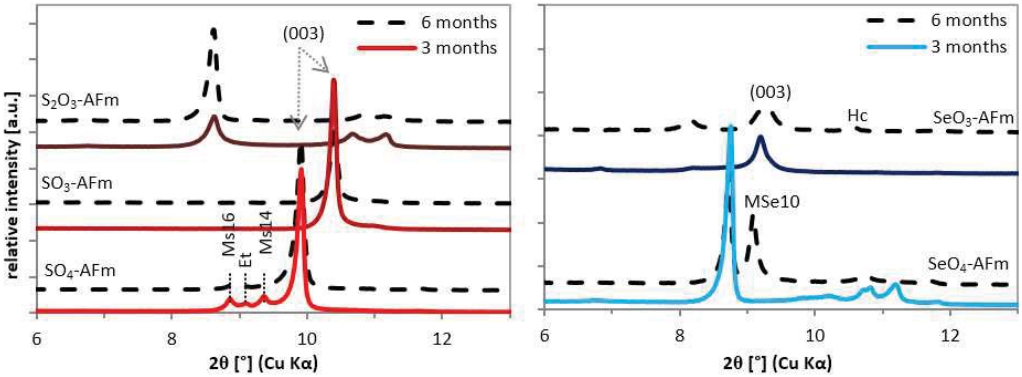


***Figure 5:*** *XRD-pattern of the synthesized AFm phases (pH ~ 13) after 3 and 6 months (dotted line) equilibration time and drying over a saturated NaOH-solution (r.h. ~ 10%). MSe10: $SeO_4$-AFm with 10 $H_2O$.*

### *Effect of lower pH*

$SO_4$- and $SeO_3$-AFm phases were also synthesized using Ca-salt instead of Na-salts as a starting material resulting in a pH of ~ 12. The total amount of water loss for the lower pH samples does not differ significantly from the high pH ones and sums up to 12 $H_2O$ corresponding to 34.2 wt.% for the $SO_4$-AFm and 11 $H_2O$ corresponding to 33.2 wt.% for the $SeO_3$-AFm, respectively. The XRD-patterns are similar to those of the high pH samples (Figure 6). The main difference can be observed for the $SeO_3$-AFm which shows higher intensities of the (hkl 003)-band, which suggests increased stacking of layers. The $SO_4$-AFm has additional, small intensity peaks near the (hkl 003)-reflex indicating the presence of hemicarbonate impurities.

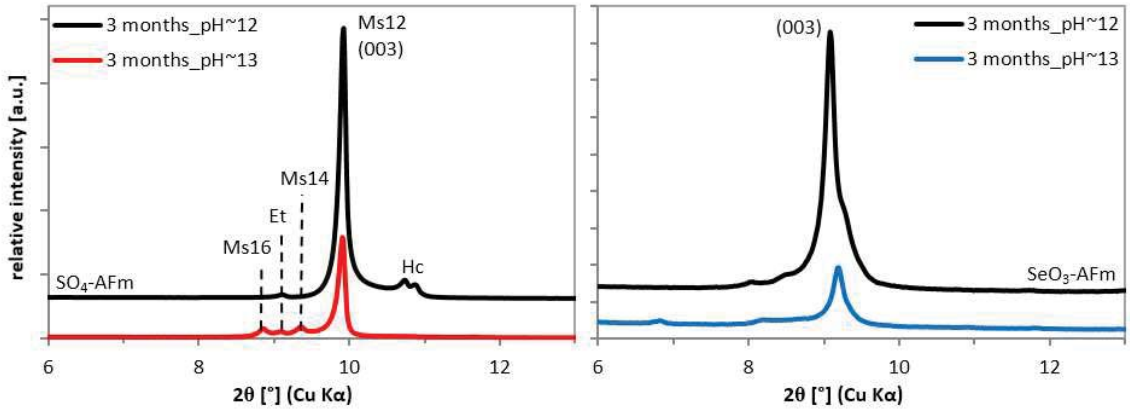


***Figure 6:*** *XRD-pattern for the $SO_4$- and $SeO_3$-AFm phases comparing the effect of pH. All samples were dried over a saturated NaOH-solution (r.h. ~ 10%).*

*Solubility products*

The measured concentrations of calcium, sodium, aluminium, sulfur and selenium in the liquid phase in equilibrium with the solids were used to calculate the solubility products using GEMS (Kulik et al., 2013), including a full speciation calculation. The activity coefficients of the aqueous species were calculated with the built-in extended Debye-Hückel equation. The results are plotted in Figure 7 together with available published data. The solubility products refer to $Ca^{2+}$, $AlO_2^-$, $OH^-$, $H_2O$, $S_2O_3^{2-}$, $SO_3^{2-}$, $SO_4^{2-}$, $SeO_4^{2-}$ and $SeO_3^{2-}$, respectively and 4 Ca within the main layer (e.g., $K_{s0}(SO_4\text{-AFm}) = \{Ca^{2+}\}^4\ \{AlO_2^-\}^2\ \{SO_4^{2-}\}\ \{OH^-\}^4\ \{H_2O\}^{12}$ for $C_4AsH_{14}$). The obtained results for the $SO_4$- and the $SeO_4$-AFm are in good agreement with the literature data (Matschei et al., 2007; Baur and Johnson, 2003b; Zhang, 2000). The slightly lower solubility products of the $SO_4$- and $SeO_4$-AFm in comparison to the solubility products of the $SO_3$- and $SeO_3$-AFm indicate that $SO_4$- and $SeO_4$-AFm tend to be more stable than $SO_3$- and $SeO_3$-AFm phases.

The calculated solubility products after 6 months are comparable to those after 3 months, although some scatter is observed. The solubility products obtained for the $SeO_3$-AFm phase at pH ~ 12 are comparable to the results obtained in the presence of 0.2 M Na and pH ~ 13. The apparent higher solubility products obtained for the $SO_4$-AFm at pH 13 could be due to the presence of a solid solution between hydroxide and sulfate as discussed in detail in Matschei et al. (2007). A part of the $OH^-$ is incorporated with the $SO_4^{2-}$ in the interlayer of the AFm which leads to apparent higher solubility products at high pH values, if referred to $SO_4$-AFm only.

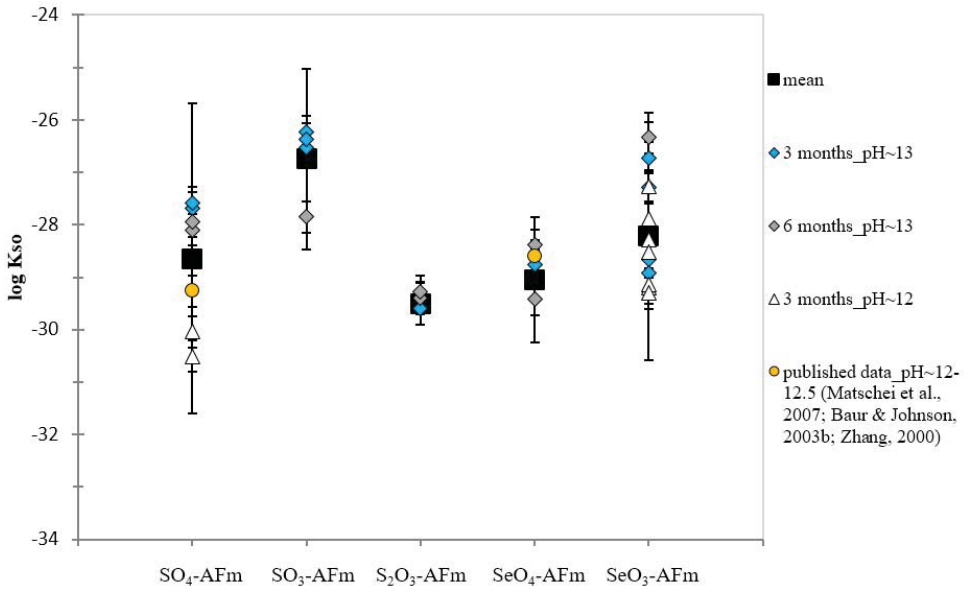


***Figure 7:*** *Solubility products of AFm phases from the present work and reported in literature (Matschei et al., 2007; Baur and Johnson, 2003b; Zhang, 2000) comparing the effect of time and pH. Calculated error on the mean values indicates the 95% confidence interval.*

## Conclusions and future work

In this study the formation of AFm phases with reduced sulfur and selenium species - S(IV), S(II) and Se(IV) - was investigated. All synthesized products show a crystalline structure with rhombohedral or monoclinic symmetry. The S(IV)- and the Se(IV)-AFm have an identical position of the main layer reflection (hkl 110) as the S(VI)-AFm, indicating also a rhombohedral structure. Different interlayer distances (hkl 003 and 006) for these

two phases are observed as a function of the size of the interlayer anions and/or the number of water molecules present in the interlayer. The S(II)- and the Se(VI)-AFm show a lower symmetry consistent with a monoclinic structure. TGA displays typical water loss pattern of AFm phases with a water content of 11 $H_2O$ for the $SO_3$- and the $SeO_3$-AFm, 12 $H_2O$ molecules for the $SO_4$-AFm, and 13 $H_2O$ for the $S_2O_3$- and the $SeO_4$-AFm.

Longer equilibration times lead to more stacking of layers resulting in higher intensities of the reflection related to the basal spacing on a XRD spectrum.

Future objectives are:

- Synthesis and characterization of binary AFm solid solutions containing various ratios of Se(VI), Se(IV), I(-I), and $X^{n-}$ with $X^{n-} = SO_4^{2-}$, $SO_3^{2-}$, $S_2O_3^{2-}$, $CO_3^{2-}$, $OH^-$
- Synthesis and characterization of S(-II)-AFm ($HS^-$-AFm) and Se(-II)-AFm ($HSe^-$-AFm)
- Construction of thermodynamic models describing the above-mentioned solid solutions using GEMS, taking into account the observed uncertainties.

## Acknowledgement

*The research leading to these results has received funding from the European Union's Horizon 2020 Research and Training Programme of the European Atomic Energy Community (EURATOM) (H2020-NFRP-2014/2015) under grant agreement n° 662147 (CEBAMA).*

*The authors would like to acknowledge Professor Guillaume Renaudin (SIGMA-Clermont, France) for his work on the crystal structure analyses.*

## References

Allmann, R. (1977). Refinement of the hybrid layer structure. Neues Jahrbuch für Mineralogie-Monatshefte, 3, 136-144.

Baquerizo, L.G., Matschei, T., Scrivener, K.L., Saeidpour, M., Wadsö, L. (2015). Hydration states of AFm cement phases. Cement and Concrete Research, 73, 143-157.

Baur, I. and Johnson, C.A. (2003a). Sorption of selenite and selenate to cement minerals. Environmental Science & Technology, 37, 3442-3447.

Baur, I. and Johnson, C.A. (2003b). The solubility of selenate-AFt ($3CaO{\cdot}Al_2O_3{\cdot}3CaSeO_3{\cdot}37.5H_2O$) and selenate-AFm ($3CaO{\cdot}Al_2O_3{\cdot}CaSeO_4{\cdot}xH_2O$). Cement and Concrete Research, 33, 1741-1748.

Bonhoure, I., Baur, I., Wieland, E., Johnson, C.A., Scheidegger, A.M. (2006). Uptake of Se(IV/VI) oxyanions by hardened cement paste and cement minerals: An X-ray absorption spectroscopy study. Cement and Concrete Research, 36, 91-98.

Dilnesa, B.Z., Lothenbach, B., Le Saout, G., Mesbah, A. Filinchuk, Y. Wichser, A., Wieland, E. (2011). Iron in carbonate containing AFm phases. Cement and Concrete Research, 41, 311-323.

Evans, D.G. and Slade, R.C.T. (2006). Structural aspects of layered double hydroxides. *In:* Duan, X. and Evans, D.G. (Eds.) Layered Double Hydroxides. Springer-Verlag, 119, 1-87.

Kulik, D.A., Wagner, T., Dmytrieva, S.V., Kosakowski, G., Hingerl, F.F., Chudnenko, K.V., Berner, U. (2013). GEM-Selektor geochemical modeling package: revised algorithm and GEMS3K numerical kernel for coupled simulation codes. Computational Geosciences, 17, 1-24.

Mace, N., Landesman, C., Pointeau, I., Grambow, B., Giffaut, E. (2007). Characterisation of thermally altered cement pastes. Influence on selenite sorption. Advances in Cement Research, 19, 157-165.

Matschei, T., Lothenbach, B., Glasser, F.P. (2007). The AFm phase in Portland cement. Cement and Concrete Research, 37, 118-130.

Motzet, H. and Pöllmann, H. (1999). Synthesis and characterization of sulfite-containing AFm phases in the system $CaO$-$Al_2O_3$-$SO_2$-$H_2O$. Cement and Concrete Research, 29, 1005-1011.

NAGRA (2002). Project Opalinus Clay. Safety report. Demonstration of disposal feasibility for spent fuel, vitrified high-level waste and long-lived intermediate level waste. Nagra Technical Report, NTB 02-05.

Olin, Å., Noläng, B., Osadchii, E.G., Öhman, L.-O., Rosén, E. (2005). Chemical thermodynamics of Selenium. Elsevier.

Puigdomenech, I. (1983). INPUT, SED, and PREDOM: Computer programs drawing equilibrium diagrams. TRITA-OOK-3010. Royal Institute of Technology (KTH), Dept. Inorg. Chemistry, Stockholm, Sweden.

Renaudin, G., Segni, R., Mentel, D., Nedelec, J.M., Leroux, F., Taviot-Gueho, C. (2007). A Raman study of the sulfated cement hydrates: ettringite and monosulfoaluminate. Journal of Advanced Concrete Technology, 5, 299-312.

Vernet, C. (1982). Comportement de l'ion $S^{2-}$ au cours de l'hydratation des ciments riches en laitier (CLK). Formation de solutions solides de $S^{2-}$ dans les aluminates hydrates hexagonaux. Silicates Industriels, 3, 85-90.

Zhang, M. (2000). Incorporation of oxyanionic B, Cr, Mo, and Se into hydrocalumite and ettringite: Application to cementitious systems. PhD Thesis at the University of Waterloo, Ontario, Canada.